ARTICLES
PUBLISHED ONLINE: 1 FEBRUARY 2016 | DOI: 10.1038/NMAT4552
nature materials

Conductance saturation in a series of highly transmitting molecular junctions

T. Yelin[1], R. Korytár[2], N. Sukenik[1], R. Vardimon[1], B. Kumar[3], C. Nuckolls[3], F. Evers[2] and O. Tal[1]*

Revealing the mechanisms of electronic transport through metal–molecule interfaces is of central importance for a variety of molecule-based devices. A key method for understanding these mechanisms is based on the study of conductance versus molecule length in molecular junctions. However, previous works focused on transport governed either by coherent tunnelling or hopping, both at low conductance. Here, we study the upper limit of conductance across metal–molecule–metal interfaces. Using highly conducting single-molecule junctions based on oligoacenes with increasing length, we find that the conductance saturates at an upper limit where it is independent of molecule length. With the aid of two prototype systems, in which the molecules are contacted by either Ag or Pt electrodes, we find two different possible origins for conductance saturation. The results are explained by an intuitive model, backed by *ab initio* calculations. Our findings shed light on the mechanisms that constrain the conductance of metal–molecule interfaces at the high-transmission limit.

Understanding the properties of electronic transport across metal–molecule interfaces is essential for controlling a large variety of molecular-based devices such as organic light-emitting diodes[1], nanoscale organic spin valves[2] and single-molecule switches[3]. One of the primary experimental methods to reveal the mechanisms behind electronic transport through metal–molecule interfaces is the study of conductance as a function of molecule length in molecular junctions[4–13]. Previous studies focused on transport at the coherent tunnelling or hopping regimes, both characterized by low conductance. However, the upper limit of conductance across molecular junctions has not been explored, despite the great potential for efficient information transfer, charge injection and recombination processes at high conductance. To study the conductance characteristics of highly transmitting molecular junctions, strong electronic coupling is required between the molecule and the electrodes, as well as within the molecule itself[9,10,14,15]. These conditions are achieved in this work by direct hybridization between the π-orbitals of oligoacene molecules and the frontier orbitals of metal electrodes, without employing anchoring groups such as thiols that can act as spacers between the orbitals of the molecular backbone and the frontier orbitals of the metal[13,14]. The oligoacenes (Fig. 1a) are linear π-conjugated molecules that can be viewed as short graphene nanoribbons[16], whose electronic structure is subject to ongoing research[17]. Here, we study the evolution of conductance as a function of molecule length and compare the conductance characteristics of two prototype systems based on either Ag or Pt electrodes. Whereas Ag has mainly frontier *s*-orbitals available for conductance, Pt has also prominent frontier *d*-orbitals. Ag/oligoacene junctions yield a non-trivial conductance trend, where the conductance first increases with molecule length, followed by the onset of conductance saturation. For these molecular junctions, the conductance saturation is ascribed to a competition between energy level alignment and level broadening. Conversely, the conductance of Pt/oligoacene junctions is approximately equal to the conductance quantum ($G_0 = 2e^2/h \approx 12.9\,\mathrm{k\Omega}^{-1}$) and does not depend on the molecule length. The conductance saturation in this case is attributed to a robust band-like transport. Our analysis indicates that Ag-based molecular junctions preserve the fingerprint of the electronic structure of the molecules and serve as a probe for the interplay between level alignment and electrode–molecule coupling strength. In contrast, for Pt-based junctions, the molecular energetic features are smeared out owing to significant π-*d* hybridization, leading to high conductance, which is insensitive to variations in the molecular level structure. These findings pave the way for controlled electronic transport at the high-transmission limit by manipulating the orbital hybridization at metal–molecule interfaces.

Experiments are performed in a break-junction set-up[18] (Fig. 1a) at cryogenic temperatures (~4.2 K). Two freshly exposed electrodes are formed by controllably breaking a metal wire into two segments, separated by a gap that can be adjusted in sub-atomic resolution. Before introducing the molecules, the typical conductance of the metal atomic junction is analysed by recording conductance traces as a function of the relative electrode displacement, as shown for Ag junction in Fig. 1b, left panel. When the electrodes are pulled apart, the contact is narrowed, and the conductance decreases ('pull' conductance traces, blue). The conductance plateaux at $\sim 1G_0$ correspond to a single Ag atom at the smallest cross-section[19,20], where further stretching leads to junction rupture. Following the rupture of the junction, the electrodes are pushed together and the conductance increases as the contact is reformed ('push' conductance traces, red). To characterize the key conductance features, conductance histograms are constructed from thousands of traces. Figure 1c, left panel, reveals peaks at $\sim 1G_0$ that correspond to the most probable conductance value of the Ag atomic junction. The tail at low conductance is the signature of tunnelling transport measured immediately after rupture or before reforming a contact[20,21]. The conductance–displacement density plots in Fig. 1c, middle and right panels show the conductance evolution when pulling or pushing the electrodes, respectively.

In a series of independent experiments, oligoacene molecules (benzene, naphthalene, anthracene…) are introduced, one type

[1]Chemical Physics, Weizmann Institute of Science, 7610001 Rehovot, Israel. [2]Institut für Theoretische Physik, Universität Regensburg, D-93053 Regensburg, Germany. [3]Department of Chemistry, Columbia University, New York 10027, USA. *e-mail: oren.tal@weizmann.ac.il

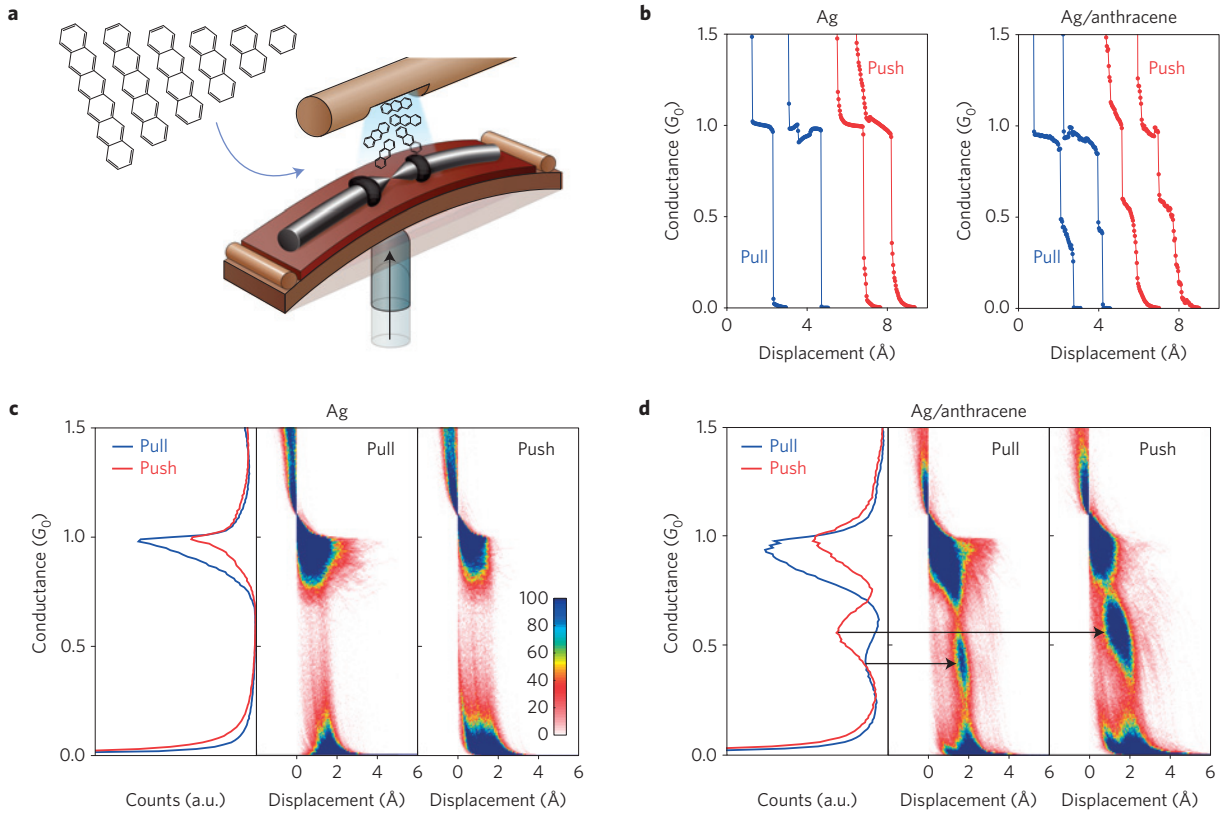

Figure 1 | Characterization of Ag/oligoacene molecular junctions. a, Illustration of a break-junction set-up and the structure of the studied series of oligoacene molecules (right to left: benzene, naphthalene, anthracene, tetracene, pentacene, hexacene). **b**, Pull (blue) and push (red) conductance traces of Ag (left panel) and Ag/anthracene (right panel). **c**, Characterization of Ag atomic junctions. Left panel: pull (blue) and push (red) conductance histograms. Middle and right panels: conductance–displacement density plots constructed from pull and push conductance traces, respectively. **d**, The same characterization for Ag/anthracene molecular junctions. The histograms and the density plots are composed from at least 5,000 traces, recorded at a bias voltage of 100 mV. Zero displacement is set for each trace as the first displacement point with a conductance value below $1.1G_0$. Push values are typically higher than pull values, probably owing to induced elongation of the bonds in the pulling process that suppresses the conductance.

of oligoacenes at each experiment, to a bare Ag junction from a molecular source (Fig. 1a). As an example, typical conductance traces for Ag/anthracene molecular junctions are shown in Fig. 1b, right panel. Here, additional tilted plateaux can be seen following the typical conductance plateaux of the Ag atomic junctions. The corresponding conductance histograms are shown in Fig. 1d, left panel. The peak at $\sim 1G_0$ is still apparent; however, another peak is observed at lower conductance, indicating the formation of molecular junctions. The association of the lower peak with molecular junctions was verified by inelastic electron spectroscopy (IES) measurements (Supplementary Section 1). In the density plots (Fig. 1d, middle and right panels), the formation of molecular junctions is indicated by the new spots appearing below the typical conductance of the Ag junction. Owing to the lack of specific binding groups, determining the exact binding geometries is not trivial. However, useful information about the structure of the junctions can be extracted by examining the length of the molecular conductance features. The short molecular features seen in the density plots indicate a very limited elongation of the molecular junctions, which is even shorter than the elongation of the Ag atomic contact at $\sim 1G_0$. Analysis of individual traces (for example, Fig. 1b) shows that the lengths of the tilted plateaux, which correspond to the elongation of the molecular junctions, do not exceed 1–2 Å. This minor elongation indicates that the molecule is oriented in a compact configuration, with its long axis pointing out of the junction (exemplified in the calculations below). Tilting or sliding of the molecule into a longitudinal configuration, in which the molecule would be attached to the electrodes through its long ends (for example, Supplementary Fig. 4, inset) is inconsistent with the short molecular features[22]. Remarkably, the different molecular junctions along the Ag/oligoacene series reveal the same junction elongation regardless the length of the molecule (Supplementary Figs 2 and 3). This observation further verifies the conclusion that the molecules are positioned with their short axes touching the electrodes, yielding molecular junctions with similar total elongation regardless the molecule length. This configuration allows us to study the influence of the energetic variations due to the molecule length while avoiding the effect of the increased length of the conducting bridge along the series. A thorough analysis of the Ag/oligoacene junction geometry appears in Supplementary Section 2.

The characteristic conductance of each Ag/oligoacene molecular junction, determined from the peaks in the conductance histograms, is presented in Fig. 2. Typical conductance histograms for the different Ag/oligoacene junctions are presented in Supplementary Fig. 7. Out of the six molecules studied, five showed a clear peak in the conductance histograms. As seen in Fig. 2, the conductance trend along the Ag/oligoacene series is composed of two main regions. Initially, the conductance increases with molecule length. However, beyond three rings the onset of conductance saturation can be observed. Although an increase in conductance with molecule length had been previously reported[6,10], this is the first time that saturation of conductance at an upper value has been observed.

To study the origin of the conductance trend along the Ag/oligoacene series, we performed *ab initio* transport calculations

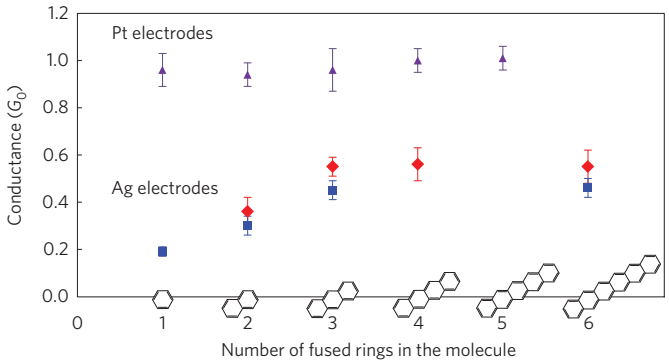

Figure 2 | The characteristic conductance of Ag/oligoacene and Pt/oligoacene junctions as a function of molecule length. The molecule length is expressed as the number of benzene rings in the oligoacene molecule. Lower series: The characteristic conductance of Ag/oligoacene junctions, determined from the peaks in the pull (blue square) and push (red diamond) conductance histograms. All the studied molecules except the pentacene showed a clear conductance peak in either pull or push directions. Upper series: The characteristic conductance of Pt/oligoacene junctions, determined from the peaks in the pull conductance histograms (purple triangle). Values from push histograms (not presented) are typically higher by ~0.02–0.1G_0. Error bars represent the standard deviation between independent experiments. For more information see Supplementary Section 3.

(see Methods section) for a variety of junction geometries. We find that different compact geometries yield qualitatively the same conductance trend as observed in the experiments. Figure 3a presents transmission curves for the compact configuration demonstrated in the inset. Another example for a compact configuration can be found in Supplementary Fig. 5. We note that calculations for a longitudinal junction configuration (Supplementary Fig. 4) yield a very different transmission trend than the experimentally observed one. These observations support the length analysis indications for junction geometries that are limited to a set of compact configurations. According to our calculations (for example, Fig. 3a), the conductance, determined by the value of the transmission curves at the Fermi energy E_F, is dominated by the lowest unoccupied molecular orbitals (LUMOs), which are much closer to E_F than the highest occupied molecular orbitals (HOMOs). The difference between the transmission values at E_F diminishes with molecule length, implying the onset of conductance saturation. The transmission peaks can be approximated by Lorentzians—except for the benzene peak, owing to a twofold LUMO degeneracy. The evolution of the LUMO peaks with molecule length indicates two trends with competing effects on the conductance. The first is a reduction in the separation between E_F and the peak centre ε (Fig. 3b, red), which acts to increase the conductance; the second is a reduction in the peak width Γ (Fig. 3b, blue), which acts to decrease the conductance. These trends along the series of molecular junctions are robust and occur for different junction configurations, implying a general behaviour that is independent of a specific configuration.

Despite the complexity of molecular junctions, intuition about these two trends can be obtained from simple physical considerations, based on the length of the oligoacene molecules and their conjugated nature. In analogy to a 'particle in a box' (Fig. 4a), the HOMO–LUMO gap of the oligoacenes, related to ε, is reduced with molecule length[23]. In this context, ε can be approximated by: $\varepsilon \propto (2n+1)/N^2$, where the molecule length is expressed by N, the number of benzene rings comprising the molecule. Here, n stands for the quantum number of the molecular π-orbital that dominates the conductance. The quantum number n increases with the number of π-electrons and is therefore proportional to N. This results in

$$\varepsilon = c_1/N + c_2/N^2 \quad (1)$$

where c_1, c_2 are constants. The energies of the molecular levels can be modified considerably when the molecule is suspended between metal electrodes. However, the general tendency of reduction in the HOMO–LUMO gap with length is preserved[4,7,10,24], implying a better alignment of these orbitals with E_F, and an increase of conductance. To understand the onset of saturation that follows the conductance increase, it is important to consider another factor, the broadening Γ of the LUMO peak, which results from the coupling of the LUMO to the extended states of the electrodes[1,24]. Because the molecular π-orbitals are delocalized over the whole molecule, the electron density per orbital decreases with molecule length as $\sim 1/N$ (Fig. 4b). When the molecule is attached to the metal electrodes, the molecular wavefunctions are modified. However, in a simplified picture, when the $1/N$ dependence remains dominant,

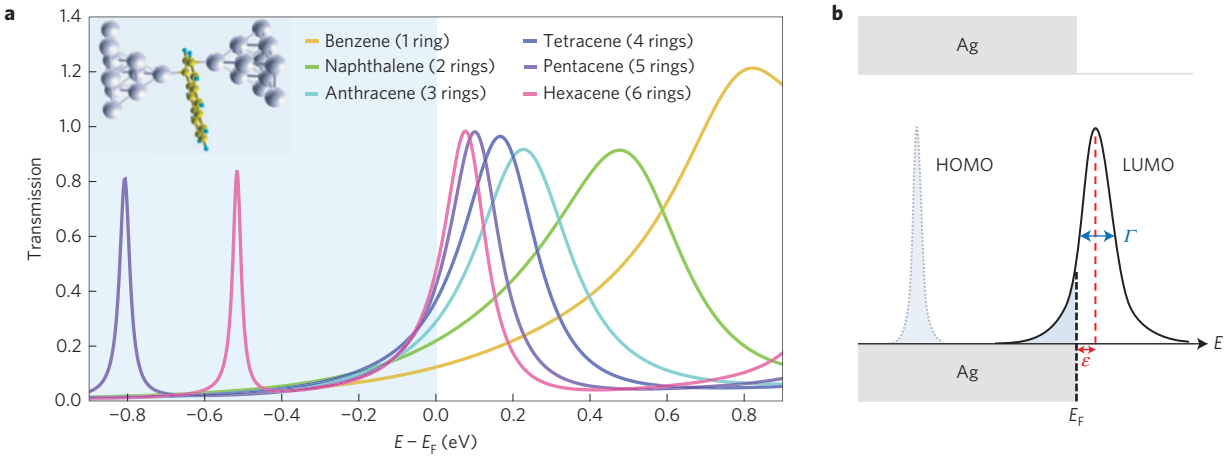

Figure 3 | Calculated transmission curves and the corresponding single-Lorentzian model for the Ag/oligoacene junctions. a, Calculated transmission curves for a series of Ag/oligoacene junctions, with a compact junction configuration demonstrated for Ag/anthracene in the inset. The conductance of each junction is determined by the transmission value at E_F, which is dominated by the LUMO-type peaks, centred at energies higher than E_F. **b**, Illustration of ε (red), the energetic distance between the centre of the peak and E_F, and of Γ (blue), the energetic width of the peak in the framework of a single-Lorentzian LUMO-type transmission resonance that determines the conductance.

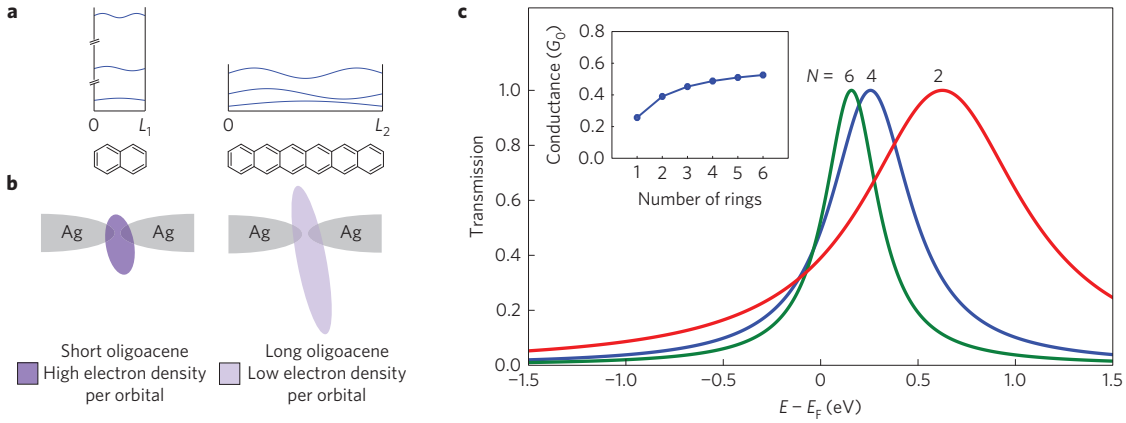

Figure 4 | A single-level model explaining the conductance trend along the Ag/oligoacene series. a, A 'particle in a box' analogy for the energy level spacing of the oligoacenes. Increasing molecule length leads to a decrease in the energy level spacing. **b**, Schematic illustration of the electron density per π-orbital, demonstrated by the colour intensity. The density decreases with molecule length, because the orbitals are spread over the whole molecule. This results in a lower overlap of the orbital with the valence orbitals at the apices of the electrodes. **c**, A reconstruction of a conductance trend which is similar to the measured conductance trend along the Ag/oligoacene series by equation (3) (fitting parameters: $c_a = 0.8$, $c_b = 0.9$) and examples for the corresponding calculated Lorentzian LUMO peaks for representative molecule length ($N = 2,4,6$).

the overlap of the LUMO with the frontier metal orbitals decreases accordingly, yielding

$$\Gamma = c_3/N \tag{2}$$

where c_3 is a constant. The reduction in Γ with molecule length acts to decrease the conductance, as opposed to the reduction in ε which acts to increase the conductance.

The resulting conductance trend is determined by the interplay between ε and Γ, as evident from the expression for conductance in the single-Lorentzian model[25]: $G = G_0/[(\varepsilon/\Gamma)^2 + 1]$. By introducing equations 1 and 2, this expression is reduced to:

$$G = G_0/[(c_a + c_b/N)^2 + 1] \tag{3}$$

where $c_a = c_1/c_3$ and $c_b = c_2/c_3$. For short molecules the conductance increases with molecule length. However, for long enough molecules (large N) the term c_b/N becomes negligible and the conductance saturates (G is independent of N). In Fig. 4c, inset, equation (3) is used to reconstruct a conductance trend, which is similar to the experimental one. The corresponding Lorentzian transmission peaks for representative molecule lengths ($N = 2,4,6$) are shown in Fig. 4c, demonstrating conductance increase ($2 \rightarrow 4$) and the onset of conductance saturation ($4 \rightarrow 6$). We note that the molecule length at the onset of saturation and the conductance value at saturation would depend on the specific junction geometry. Interestingly, in our case, the conditions for the onset of saturation are already met for $N = 3$. The success of our minimal model in using the interplay between ε and Γ to capture the essential features of the measured conductance suggests that the onset of conductance saturation can be explained by simple physical considerations.

As long as a single-level model applies, the (dimensionless) ratio ε/Γ indicates not only the conductance but also the charge transfer between the electrodes and the involved molecular level. According to Friedel's sum rule, the conductance can be expressed uniquely through the charging of the level q by $G = G_0 \sin^2((\pi/2)q)$ (see Supplementary Section 5). The relation shows that the saturation of conductance, which is a non-equilibrium quantity, is correlated with the saturation of charge, which is an equilibrium quantity. Thus conductance saturation at $G \sim 0.5$–$0.6G_0$ is associated with charge transfer of $q \sim 0.5$–0.6 electrons to the LUMO. In view of the above, the conductance saturation can be modelled even in situations where deviations from the presented approximations take place—for example, when the assumptions derived from a 'particle in a box' do not apply or when ε is not proportional to the HOMO–LUMO gap.

In principle, our model can be verified by transport measurements incorporating electrostatic gating abilities[26]. By electrostatically lowering (raising) the energy of the LUMO, the charging of the level q should increase (decrease), and so should the conductance. This should result in a shift of the conductance saturation point, because the ε/Γ ratio will be modified. An additional verification for the model could be obtained by extracting ε and Γ from I–V measurements[27–29] to track the evolution of these parameters as a function of molecule length. In the examined case, owing to the very broad resonances, a very large voltage window is needed to extract these parameters from the nonlinear regime of the I–V curves. As a result of the high conductance and the limited metal–molecule bond strength of our junctions, applying a high voltage leads to instabilities, probably related to Joule heating[30,31]. Obtaining a different series of molecular junctions that are characterized by similar conductance properties, yet with stronger metal–molecule bonds, may allow stable I–V measurements in a wide enough voltage window to independently test our model.

A remarkably different conductance behaviour is observed when similar experiments are performed using Pt electrodes, which in contrast to Ag have prominent valence d-orbitals available for conductance. As shown in Fig. 2 (upper purple triangles), the series of Pt/oligoacenes has a very high characteristic conductance of $\sim 1G_0$. The attribution of this conductance to molecular junctions[32,33] is verified by IES measurements (Supplementary Section 1). Figure 5a shows that this conductance appears below the typical conductance of Pt atomic junctions, found at $\sim 1.5G_0$ (refs 34,35). The molecular conductance at $\sim 1G_0$ is independent of the molecule length, namely conductance saturation along the entire series. This saturation, however, has a different origin from that observed for the Ag/oligoacene system. Previous studies have found that the type of the metal electrode can change the conductance of the molecular junction[7,8]. However, in all these cases, the conductance trends as a function of molecule length were not considerably modified. Here, the two sets of oligoacene-based molecular junctions (Fig. 2) show substantially different conductance trends.

To study the origin of the insensitivity of conductance to molecule length in the Pt/oligoacene junctions, we compare the

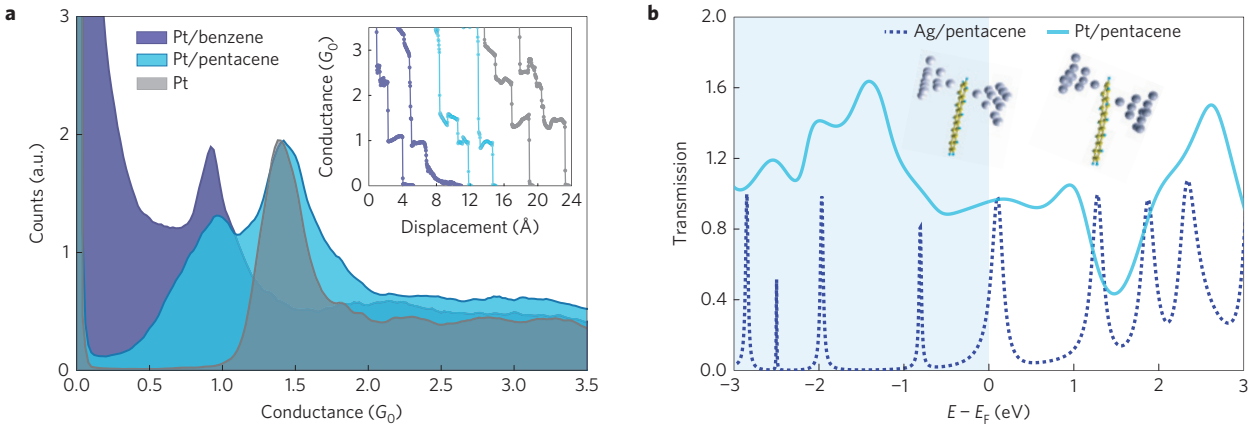

Figure 5 | Experimental and theoretical conductance characterization of the Pt/oligoacene molecular junctions. a, Conductance traces (inset) and conductance histograms recorded during pulling of Pt/benzene (purple) and Pt/pentacene (light blue), compared to bare Pt (grey). After introducing oligoacenes to the Pt junction, a characteristic peak at ~1G_0 appears, alongside or replacing the characteristic peak of the bare Pt at ~1.5G_0. Each histogram is composed of at least 5,000 traces, recorded at a bias voltage of 200 mV. **b**, Calculated transmission curve of Pt/pentacene (light blue), showing a band-like plateau of high transmission, reflecting insensitivity of the conductance to the exact location of E_F. In comparison, the transmission curve of Ag/pentacene (dashed blue) is composed of resonances that originate from the molecular levels and the conductance is sensitive to the alignment of the LUMO resonance with E_F. Inset: the junction configurations for which the transmission curves are calculated. The same inter-electrode distance (5.52 Å) is considered for the two junctions. The carbons closest to the electrode apex are 1, 3 and 1, 5 for the Ag- and Pt-based junctions, respectively.

calculated transmission curves of Ag/pentacene and Pt/pentacene (Fig. 5b). We note that similar results were obtained for other oligoacenes. The transmission curve of Ag/pentacene (dotted blue) is composed of separate resonances, originating from the molecular levels. Therefore, the conductance is determined by the width and position relative to E_F of the relevant molecular level (LUMO). On the other hand, the transmission curve of Pt/pentacene (light blue) reveals a band-like transmission in which the molecular features are smeared out, creating a broad plateau of high transmission. The conductance is then considerably less sensitive to changes in the molecular level alignment with respect to E_F. This can explain the approximately constant conductance that does not follow the variations in the electronic structure of the oligoacenes along the series. The smearing of the molecular features indicates a significant hybridization between the frontier orbitals of Pt and the conductive molecular orbitals. This observation is supported by previous calculations that found significant hybridization between the d-orbitals of Pt and the molecular π-orbitals in similar systems[33,36], and by the mechanical stability of Pt/oligoacene junctions, which is comparable to that of bare Pt atomic junctions[33]. The dominant role of the d-orbitals in the Pt case is also demonstrated in Supplementary Fig. 11. In the case of Ag/oligoacene junctions, owing to an insignificant contribution from d-orbitals around E_F, the transmission is mostly determined by the hybridization of the valence s-orbitals with the molecular π-orbitals (Supplementary Fig. 11) and the junction preserves better the molecular level character. Therefore, the different electronic nature of the metal electrodes results in significantly different orbital hybridization that leads to two physical origins for the saturation of conductance.

To conclude, we study the dependence of conductance on molecule length in a series of single-molecule junctions in the high-transmission regime. We find that the conductance can reach an upper limit where it is independent of molecule length. By comparing two series of molecular junctions, both based on oligoacenes with increasing length, albeit with a different metal as electrodes, we suggest two fundamental mechanisms for the emergence of conductance saturation. For Ag/oligoacene junctions, the conductance increases with molecule length, followed by the onset of conductance saturation at a value determined by the interplay between energy level alignment and electrode–molecule coupling strength. In contrast, Pt/oligoacene junctions are characterized by a band-like transmission, resulting in approximately constant conductance along the series of molecular junctions, regardless of the molecule length. Thus, by the appropriate choice of metal electrodes, one can either obtain tunability of conductance, or alternatively achieve a robust metallic-like conductance across molecular junctions. Our findings provide insights into the conductance properties of metal–molecule interfaces near the full-transmission limit, which are central for the realization of highly conductive metal–molecule interfaces.

Methods

Methods and any associated references are available in the online version of the paper.

Received 25 March 2015; accepted 21 December 2015; published online 1 February 2016

References

1. Ratner, M. A. Introducing molecular electronics. *Mater. Today* **5,** 20–27 (February 2002).
2. Rocha, A. R. *et al.* Towards molecular spintronics. *Nature Mater.* **4,** 335–339 (2005).
3. van der Molen, S. J. & Liljeroth, P. Charge transport through molecular switches. *J. Phys. Condens. Matter* **22,** 133001 (2010).
4. Quek, S. Y., Choi, H. J., Louie, S. G. & Neaton, J. B. Length dependence of conductance in aromatic single-molecule junctions. *Nano Lett.* **9,** 3949–3953 (2009).
5. Livshits, G. I. *et al.* Long-range charge transport in single G-quadruplex DNA molecules. *Nature Nanotech.* **9,** 1040–1046 (2014).
6. Quinn, J. R., Foss, F. W., Venkataraman, L., Hybertsen, M. S. & Breslow, R. Single-molecule junction conductance through diaminoacenes. *J. Am. Chem. Soc.* **129,** 6714–6715 (2007).
7. Kim, B., Choi, S. H., Zhu, X. Y. & Frisbie, C. D. Molecular tunnel junctions based on π-conjugated oligoacene thiols and dithiols between Ag, Au, and Pt contacts: effect of surface linking group and metal work function. *J. Am. Chem. Soc.* **133,** 19864–19877 (2011).
8. Kim, T., Vázquez, H., Hybertsen, M. S. & Venkataraman, L. Conductance of molecular junctions formed with silver electrodes. *Nano Lett.* **13,** 3358–3364 (2013).
9. Diez-Perez, I. *et al.* Controlling single-molecule conductance through lateral coupling of π orbitals. *Nature Nanotech.* **6,** 226–231 (2011).
10. Kaliginedi, V. *et al.* Correlations between molecular structure and single-junction conductance: a case study with oligo (phenylene-ethynylene)-type wires. *J. Am. Chem. Soc.* **134,** 5262–5275 (2012).

11. He, J. *et al.* Electronic decay constant of carotenoid polyenes from single-molecule measurements. *J. Am. Chem. Soc.* **127,** 1384–1385 (2005).
12. Rascón-Ramos, H., Artés, J. M., Li, Y. & Hihath, J. Binding configurations and intramolecular strain in single-molecule devices. *Nature Mater.* **14,** 517–522 (2015).
13. Cheng, Z. L. *et al. In situ* formation of highly conducting covalent Au-C contacts for single-molecule junctions. *Nature Nanotech.* **6,** 353–357 (2011).
14. Ferrer, J. & García-Suárez, V. Tuning the conductance of molecular junctions: transparent versus tunneling regimes. *Phys. Rev. B* **80,** 085426 (2009).
15. Venkataraman, L., Klare, J. E., Nuckolls, C., Hybertsen, M. S. & Steigerwald, M. L. Dependence of single-molecule junction conductance on molecular conformation. *Nature* **442,** 904–907 (2006).
16. Watanabe, M. *et al.* The synthesis, crystal structure and charge-transport properties of hexacene. *Nature Chem.* **4,** 574–578 (2012).
17. Korytár, R., Xenioti, D., Schmitteckert, P., Alouani, M. & Evers, F. Signature of the Dirac cone in the properties of linear oligoacenes. *Nature Commun.* **5,** 5000 (2014).
18. Muller, C. J. Experimental observation of the transition from weak link to tunnel junction. *Phys. C* **191,** 485–504 (1992).
19. Pauly, F. *et al.* Molecular dynamics study of the thermopower of Ag, Au, and Pt nanocontacts. *Phys. Rev. B* **84,** 195420 (2011).
20. Limot, L., Kröger, J., Berndt, R., Garcia-Lekue, A. & Hofer, W. A. Atom transfer and single-adatom contacts. *Phys. Rev. Lett.* **94,** 126102 (2005).
21. Untiedt, C. *et al.* Formation of a metallic contact: jump to contact revisited. *Phys. Rev. Lett.* **98,** 206801 (2007).
22. Kamenetska, M. *et al.* Formation and evolution of single-molecule junctions. *Phys. Rev. Lett.* **102,** 126803 (2009).
23. Murov, S. L., Carmichael, I. & Hug, G. L. *Handbook of Photochemistry* (CRC Press, 1993).
24. Moth-Poulsen, K. & Bjornholm, T. Molecular electronics with single molecules in solid-state devices. *Nature Nanotech.* **4,** 551–556 (2009).
25. Datta, S. *Quantum Transport: Atom to Transistor* (Cambridge Univ. Press, 2005).
26. Perrin, M. L. *et al.* Large tunable image-charge effects in single-molecule junctions. *Nature Nanotech.* **8,** 282–287 (2013).
27. Kim, Y., Pietsch, T., Erbe, A., Belzig, W. & Scheer, E. Benzenedithiol: a broad-range single-channel molecular conductor. *Nano Lett.* **11,** 3734–3738 (2011).
28. Zotti, L. A. *et al.* Revealing the role of anchoring groups in the electrical conduction through single-molecule junctions. *Small* **6,** 1529–1535 (2010).
29. Adak, O., Korytár, R., Joe, A. Y., Evers, F. & Venkataraman, L. Impact of electrode density of states on transport through pyridine-linked single molecule junctions. *Nano Lett.* **15,** 3716–3722 (2015).
30. Smit, R. H. M., Untiedt, C. & van Ruitenbeek, J. M. The high-bias stability of monatomic chains. *Nanotechnology* **15,** S472 (2004).
31. Huang, Z., Xu, B., Chen, Y., Ventra, M. Di & Tao, N. Measurement of current-induced local heating in a single molecule junction. *Nano Lett.* **6,** 1240–1244 (2006).
32. Kiguchi, M. *et al.* Highly conductive molecular junctions based on direct binding of benzene to platinum electrodes. *Phys. Rev. Lett.* **101,** 1–4 (2008).
33. Yelin, T. *et al.* Atomically wired molecular junctions: connecting a single organic molecule by chains of metal atoms. *Nano Lett.* **13,** 1956–1961 (2013).
34. Krans, J. M. *et al.* One-atom point contacts. *Phys. Rev. B* **48,** 14721–14724 (1993).
35. Nielsen, S. *et al.* Conductance of single-atom platinum contacts: voltage dependence of the conductance histogram. *Phys. Rev. B* **67,** 3–6 (2003).
36. Ma, G. *et al.* Low-bias conductance of single benzene molecules contacted by direct Au–C and Pt–C bonds. *Nanotechnology* **21,** 495202 (2010).

Acknowledgements

T.Y. and O.T. thank L. Goffer, B. Pasmantirer and K. L. Narasimhan for their valuable help in developing the measurement set-ups and O. Yaffe for his assistance with molecule resources. O.T. thanks the H. Perlman family for their support and acknowledges funding by the Israel Science Foundation (Grant No. 1089/15), and the Minerva Foundation (Grant No. 711136). R.K. and F.E. gratefully acknowledge the Steinbuch Centre for Computing (SCC) for providing computing time on the computer HC3 at Karlsruhe Institute of Technology (KIT). Part of the computational work was performed on the bwUniCluster resources funded by the Ministry of Science, Research and Arts and the Universities of the State of Baden-Wuerttemberg, Germany, within the framework programme bwHPC.

Author contributions

O.T. and T.Y. conceived the project and designed the experiments; T.Y. performed the experiments with assistance from N.S. and R.V.; T.Y. analysed the data; R.K. and F.E. performed the calculations and participated together with T.Y. and O.T. in the overall analysis of the results; B.K. and C.N. synthesized the final precursor for hexacene. T.Y. and O.T. wrote the paper and all co-authors commented on the manuscript.

Additional information

Supplementary information is available in the online version of the paper. Reprints and permissions information is available online at www.nature.com/reprints. Correspondence and requests for materials should be addressed to O.T.

Competing financial interests

The authors declare no competing financial interests.

Methods

Experimental. The experiments are performed using a mechanical controllable break-junction (MCBJ) set-up at 4.2 K. The sample is fabricated by attaching a notched wire of Ag (99.997%, 0.1 mm, Alfa Aesar) or Pt (99.99%, 0.1 mm, Goodfellow) to a flexible substrate (1-mm-thick phosphor-bronze covered by 100 μm insulating Kapton film). A three-point bending mechanism is used to bend the substrate to break the wire at the notch under cryogenic conditions and form an adjustable gap between two ultraclean atomically sharp tips. A piezoelectric element (PI P-882 PICMA) is used to tune the bending of the substrate and control the distance between the electrodes with sub-Åresolution. The piezoelectric element is driven by a DAQ card (NI-PCI6221 or NI-PCI4461) connected to a high-peak-current piezo driver (Piezomechanik SVR 150/1). An ensemble of junctions with diverse structures is studied by repeatedly pushing the electrodes together to form a contact of ∼50–70G_0 and pulling the electrodes apart until full rapture, using the piezo element, at a rate of 20–40 Hz, while simultaneously measuring the conductance. The junction is biased with a d.c. voltage provided by the DAQ card and divided by ten to improve the signal-to-noise ratio. The presented measurements are performed at a bias voltage range of 20–200 mV. The measured conductance does not depend on the bias voltage within this range, as demonstrated in Supplementary Fig. 9. The resulting current is amplified by a current preamplifier (SR570) and recorded by the DAQ card at a sampling rate of 50–200 kHz. The oligoacenes were purchased from Sigma-Aldrich (purity > 99.9%), except for the hexacene, which was prepared according to a published procedure[16], where the final stage of synthesis was performed *in situ* in the measurement vacuum chamber.

Calculations. Density functional theory calculations using the generalized gradient approximation to the exchange–correlation functional are performed[37]. The wavefunctions are represented in a localized basis set, as implemented in the FHI-AIMS package[38]. We use the tier2 basis set, similar to the 'double-zeta + polarization', common in quantum chemistry. On the basis of our previous findings, we perform closed shell calculations[17]. The electrodes are modelled as finite pyramidal clusters, cut from a face-centred crystal in the (111) direction. As a first step, a set of relaxed geometries is obtained by optimizing the positions of all the molecular and both apex atoms. The electrodes used for the geometry optimization contain up to 11 Ag (Pt) atoms. In the second step, the geometry is fixed and transport calculations are performed. The transmission of Kohn–Sham electrons is calculated by the non-equilibrium Green's function method for finite clusters[39] with the AITRANSS package[40]. In Ag-based junctions, the resonances are narrow (70 meV for hexacene). The conductance is thus sensitive to the level alignment. The latter is determined by screening of the excess charge. To ensure proper screening by the electrode clusters, additional layers of Ag (Pt) atoms are added to both electrodes. With Ag electrodes, only for pyramids with 101 atoms (8 layers) or more does the resonance energy of the LUMO vary by less than a few percent. With Pt electrodes, pyramids with 55 atoms (6 layers) are sufficient, because the conductance is less sensitive to shifts of the broad resonances (typical width is 1 eV, see Fig. 5b).

References

37. Perdew, J. P., Burke, K. & Ernzerhof, M. Generalized gradient approximation made simple. *Phys. Rev. Lett.* **77,** 3865–3868 (1996).
38. Blum, V. *et al. Ab initio* molecular simulations with numeric atom-centered orbitals. *Comput. Phys. Commun.* **180,** 2175–2196 (2009).
39. Arnold, A., Weigend, F. & Evers, F. Quantum chemistry calculations for molecules coupled to reservoirs: formalism, implementation, and application to benzenedithiol. *J. Chem. Phys.* **126,** 174101 (2007).
40. Bagrets, A. Spin-polarized electron transport across metal–organic molecules: a density functional theory approach. *J. Chem. Theory Comput.* **9,** 2801–2815 (2013).

nature materials

SUPPLEMENTARY INFORMATION

DOI: 10.1038/NMAT4552

Conductance saturation in a series of highly transmitting molecular junctions

T. Yelin[1], R. Korytar[2], N. Sukenik[1], R. Vardimon[1], B. Kumar[3], C. Nuckolls[3], F. Evers[2], O. Tal[1*]

1. Chemical Physics, Weizmann Institute of Science, 7610001 Rehovot, Israel, 2. Institut für Theoretische Physik, Universität Regensburg, D-93053 Regensburg, Germany, 3. Department of Chemistry, Columbia University, New York 10027, USA.

Contents

* oren.tal@weizmann.ac.il

1. Identification of molecular junction formation by inelastic electron spectroscopy

Inelastic electron spectroscopy (IES) was used in order to identify the formation of molecular junctions. As a first step, the bare metallic junctions were characterized before the introduction of molecules. Measurements of differential conductance (dI/dV) vs. applied voltage across different metallic junctions (e.g., Fig. S1a,c) showed no distinguishable features above the typical energy range of metal phonons (up to 20 meV and 25 meV for Ag and Pt, respectively)[41,42]. Following the introduction of molecules, conductance steps, which are the typical fingerprint of vibration activation in molecular junctions[32,43–46], appear in the differential conductance spectra, as exemplified in Fig. S1b,d, indicating the formation of molecular junctions.

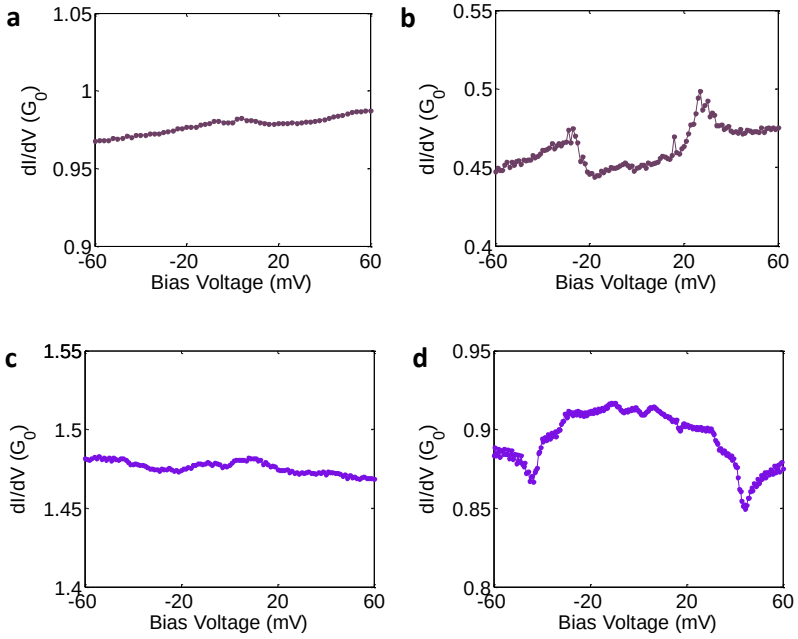

Figure S1. Examples for differential conductance spectra, used to verify the formation of molecular junctions. Differential conductance spectra of **a.** Ag atomic junction, **b.** Ag/anthracene molecular junction, **c.** Pt atomic junction, **d.** Pt/anthracene molecular junction. The spectra of the two molecular junctions show conductance steps at ~30 mV, which are associated with vibration modes of molecular junctions[32,43–46]. Note the signature of the metal phonon features around 10 mV[41,42].

2. The geometry of the Ag/oligoacene molecular junction

Different experimental and theoretical observations, which are detailed below, indicate that the Ag/oligoacene junctions are limited to an ensemble of compact configurations, in which the long axis of the molecule is pointing out of the junction, as described for example in the insets of Fig. 3a and Fig. S5a.

1. The elongation length of the molecular junctions is indicated by the tilted plateaus (e.g., Fig. 1b, right panel and Fig. S2) seen in conductance traces after the typical plateau of Ag atomic contact at ~1 G_0. These molecular plateaus end with the rupture of the junction as indicated by a clear conductance drop. Analysis of different traces shows that the typical length of the molecular plateaus and hence the molecular junction elongation is less than 1-2 Å, which is much shorter than the length of the studied molecules. The very short elongation is also seen in the analysis of large ensembles of traces presented as conductance-displacement density plots (e.g., Fig. 1d and Fig. S3). Here, the short junction elongation is indicated by the narrow spots below the conductance of the Ag atomic contact. The limited elongation is compatible with a compact junction configuration. Tilting or sliding of the molecule into a longitudinal configuration in which the molecule is suspended with its long axis approximately aligned with the junction axis (e.g., Fig. S4a, inset), would lead to a larger junction elongation in order to account for the molecule length[22,47].

2. As shown in Fig. S2 and S3, molecules with different length yield molecular conductance features of the same length, i.e., the same length of tilted plateaus in individual traces, which is manifested as spots of similar width in the density plots. This observation indicates that the molecules do not adopt longitudinal configurations. For the longitudinal configurations, the increase in molecule length along the series of molecular junctions would be manifested as an increase in the junction elongation, namely longer plateaus in the individual traces or wider spots in the density plots for the longer molecules, as was previously demonstrated[22,47]. In contrast, the fact that the elongation is remarkably similar for different molecules further supports the conclusion that the molecules adopt compact geometries for which the increasing length of the molecules along the oligoacene series has no effect on the measured junction elongation. An alternative scenario, which is based on successive changes in the contact site along the series (e.g., contacts to the same ring → contacts to neighboring rings → contacts to the 2nd neighboring rings, etc.), can be excluded as well, since such trends should also result in a detectable gradual increase in the junction length, in contrast to the experimental observation.

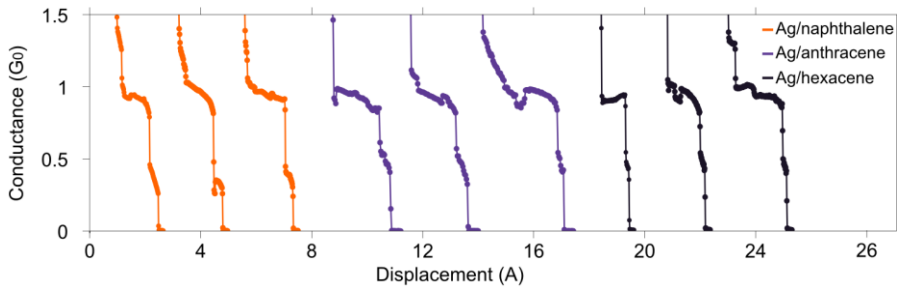

Figure S2. Conductance traces of Ag/oligoacene junctions. The molecular features (tilted plateaus), located below the plateau of the Ag atomic contact at ~1 G_0, are less than 1-2 Å in length, much shorter than the molecules. We do not observe any change in the length of the molecular features as the molecule length is increased. The traces were measured at the pull direction at bias voltage of 20-150 mV, where no voltage dependence was found.

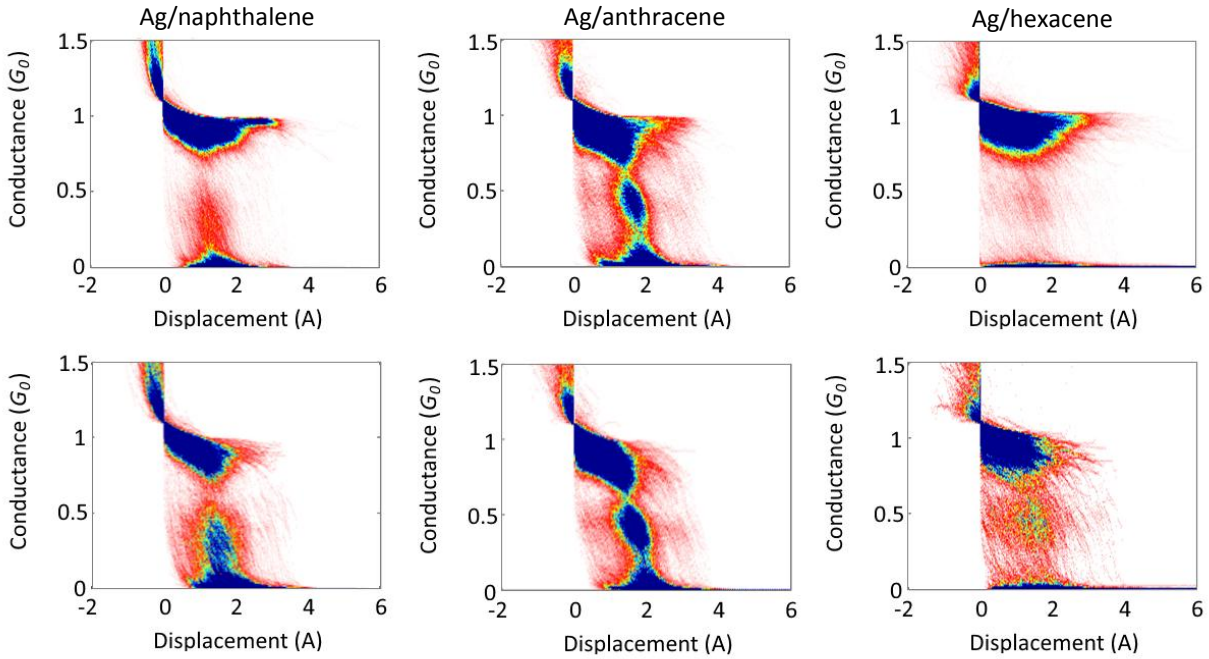

Figure S3. Conductance-displacement density plots of Ag/oligoacene molecular junctions. Upper row: Plots based on full data sets without any selection, including traces that show no indication for the formation of molecular junctions. Lower row: The corresponding plots after automatic trace selection to enhance the visibility of molecular conductance features. In these plots only traces with a non-negligible number of conductance counts (typically more than 3-5 points) at the molecular conductance range are presented. The plots are based on pull traces measured at bias voltage of 20-150 mV (for this range no voltage dependence was observed).

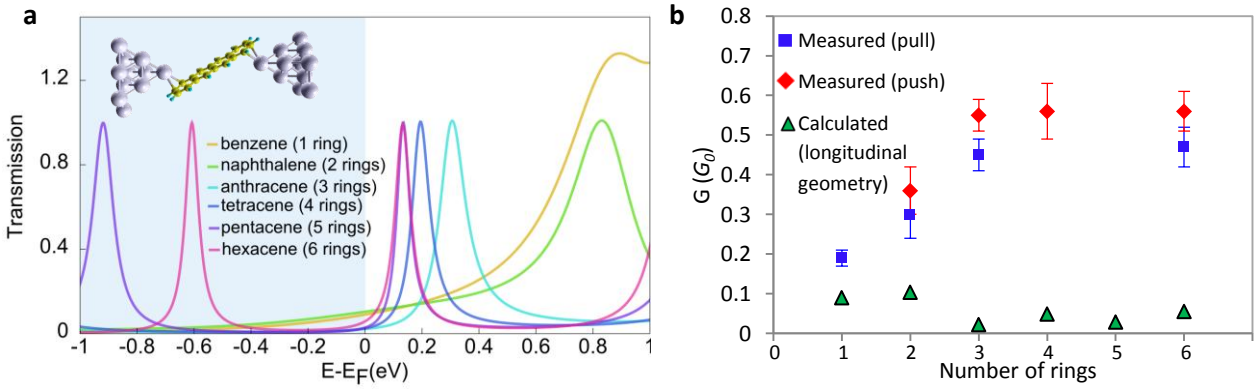

Figure S4. Calculated transmission of Ag/oligoacene junctions assuming a longitudinal configuration. a. Calculated transmission vs. energy for longitudinal Ag/oligoacene junctions. **Inset:** The configuration of the calculated junctions is illustrated for Ag/tetracene. **b**. The corresponding calculated conductance (green triangles) compared to the measured conductance for the Ag/oligoacene junctions (blue squares and red diamonds). The dependence of the measured conductance on the molecule length is in clear contrast to the trend presented by the calculated conductance assuming longitudinal junction configuration. This discrepancy indicates that the longitudinal configuration does not describe well a junction configuration, which is dominant in the experiments. The calculated trend is extracted from (a) by the value of the transmission curves at E_F.

3. Fig. S4 shows that the calculated transmission for junctions with a longitudinal geometry presents a conductance trend which is in sharp contrast to the measured conductance. This comparison supports the conclusion that longitudinal junction geometry can be excluded.

4. Transport calculations for different compact geometries give the same qualitative result, which is compatible with our experimental observations. As an example, Fig. S5 presents transmission calculations for a series of junctions with a compact configuration in which the binding to the Ag electrodes is done via neighboring rings. In this configuration the electrodes are shifted by 2.5 Å along the molecular axes, and the molecular plane tilts by ~5° compared to the configuration in Fig. 3a. The analysis of this junction geometry provides the same qualitative trends of ε (the position of the transmission peak relative to E_F) and Γ (the width of the peak) as given by our model. This observation demonstrates the robustness of our model with respect to different compact junction configurations. Transport calculations for different sets of molecular junctions that are characterized by compact geometries and diverse contact positions yield variations of 10% in ε and 20% in Γ. Beyond these moderate variations, an essential outcome that can be taken from our transport calculations for different sets of compact configurations is the preservation of the general transmission trend regardless the exact geometry. In particular according to our DFT based calculations, transport is dominated by a single transmission resonance (LUMO), which always approaches E_F with decreasing resonance width, in agreement with the proposed model in the manuscript and with the measured conductance trend.

To conclude, our experimental and theoretical analysis shows that the examined molecular junctions are limited to an ensemble of compact configurations. The only essential outcome that we take from the transport calculations is that the conductance is dominated by a single level (LUMO). In addition, our calculations indicate that the LUMO always approaches E_F while decreasing in width. This is a robust behavior (regardless the specific geometry) which gives a strong support to the model in terms of the interplay between ε and Γ.

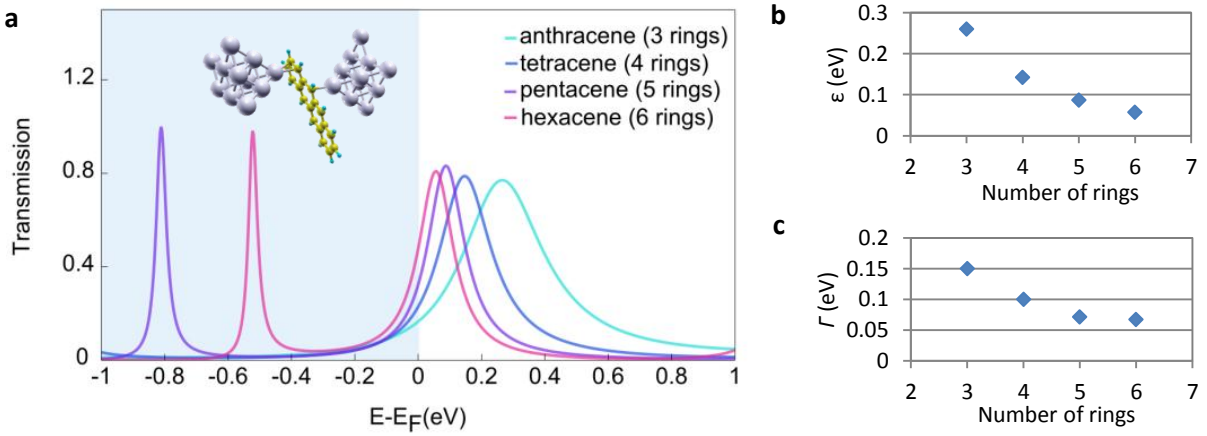

Figure S5. Analysis of calculated transmission curves for a compact configuration of the Ag/oligoacenes, where the electrodes are attached to two neighboring rings. a. Calculated transmission curves. **Inset:** The configuration of the calculated junctions is illustrated for Ag/tetracene. **b, c**. The trends of ε and Γ, respectively. The transmission curves indicate that the single level model is a good approximation (LUMO mediated conductance) and that both ε and Γ decrease with increasing molecule length, in a similar way to the case of the compact configuration shown in the main text.

An example for the effect of molecule tilting on the transmission:

In the following we compare the calculated transmission of the compact geometry presented in Fig. 3a to a similar geometry (Fig. S6), in which the molecule is constrained to lie in the plane perpendicular to the axis of the junction, yielding a tilt of approximately 12° with respect to the geometry in Fig. 3a. We note that in our experiments, the expected tilting is probably lower than 10°, according to the limited length of the measured molecular conductance plateaus. Comparing Fig. 3a to Fig. S6a, we find that the change in the molecule tilt angle results in small changes in the transmissions at E_F, while the transmission trend along the series of junctions is qualitatively the same.

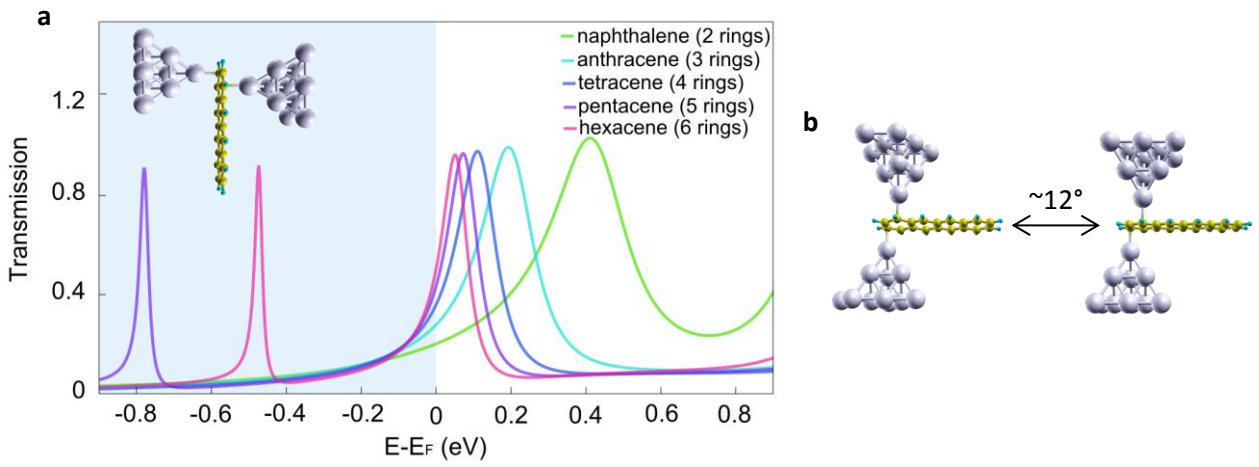

Figure S6. Calculated transmission curves for a compact unrelaxed configuration of the Ag/oligoacenes, where the plane of the molecule is perpendicular to the axis of the junction. a. Calculated transmission curves. **Inset:** The configuration of the calculated junctions is illustrated for Ag/tetracene. **b.** A comparison between the relaxed compact configuration shown in the main text (Fig. 3a) and the unrelaxed tilted configuration, with a difference of ~12° in the molecule plane. The transmission curves indicate the same qualitative transmission trend as a function of molecule length, similar to the case of the compact configuration shown in the main text.

3. Determination of the molecular junction conductance

The average typical conductance of each molecular junction was determined using the following procedure. After the introduction of molecules, a new conductance peak appeared in the conductance histograms (e.g., Fig. S7 and S8). The formation of molecular junctions at the conductance range of this conductance peak is verified by molecular vibration analysis (e.g., Fig. S1). The most probable conductance of the molecular junction is defined as the highest value of this peak. This value was determined for each conductance histogram, which is constructed from 3,000-7,000 consecutive conductance traces. We note that extracting the peak maximum by fitting a Lorentzian provides the same conductance values in the range of the experimental uncertainty. For each molecule type many conductance histograms were collected in different experimental sessions (typically 20). The typical conductance of each molecular junction type (Fig. 2) is the average value of the most probable conductance that was extracted from the entire ensemble of conductance histograms available for a specific molecule type. The error bar represents the standard deviation of this averaging.

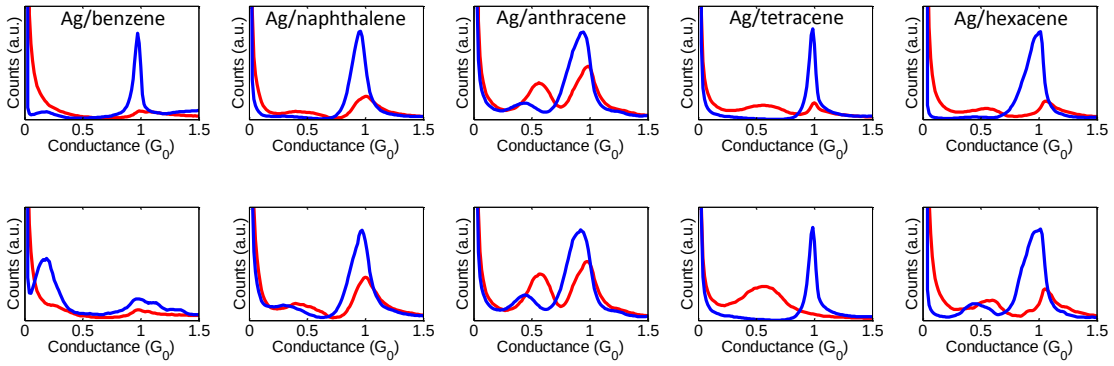

Figure S7. Conductance histograms of the different Ag/oligoacene molecular junctions. Upper row: Conductance histograms based on full data sets, consisting also traces that do not exhibit any molecular feature. Lower row: The corresponding histograms after automatic trace selection to enhance the visibility of molecular conductance peaks. In these plots only traces with a non-negligible number of conductance counts (typically more than 3-5 points) at the molecular conductance range are presented. The two methods give the same values within the error range. We note that the conductance presented in Fig. 2 in the main text is based on the full data sets without any selection. Measurements were done at a bias voltage range of 20-200 mV. The positions of the peaks are independent of bias voltage in this range, see for example Fig. S9.

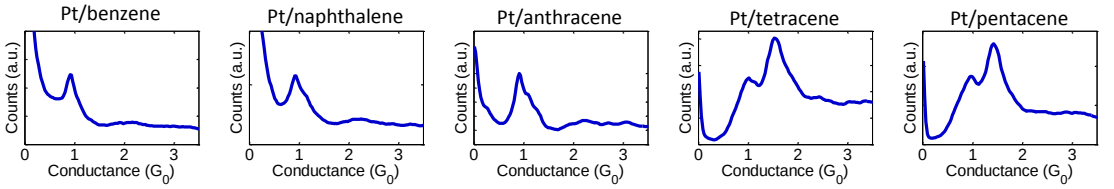

Figure S8. Conductance histograms based on pull traces for the different Pt/oligoacene molecular junctions. The peak at ~1 G_0 appears for all the junctions, while for tetracene and pentacene based junctions the peak at ~1.5 G_0, associated with Pt atomic junctions is preserved, indicating the formation of Pt atomic junctions despite the introduction of molecule to the sample. The presented histograms were measured at a bias voltage of 200 mV.

Figure S9 demonstrates the deviations between histograms of molecular junctions based on the same molecule (Ag/anthracene), measured at different bias voltages. The most probable conductance extracted from each histogram does not depend on bias voltage in the examined range.

We note that in order to study the high transmission limit for molecular junctions, linear histograms that focus on conductance values close to ~1 G_0 are used. Logarithmic histograms, such as presented in Fig. S10, were used to verify that no distinct conductance plateaus appear at the conductance range of ~0.03-0.1 G_0, which is the expected conductance of a longitudinal configuration for Ag/oligoacenes according to our calculation (Fig. S4).

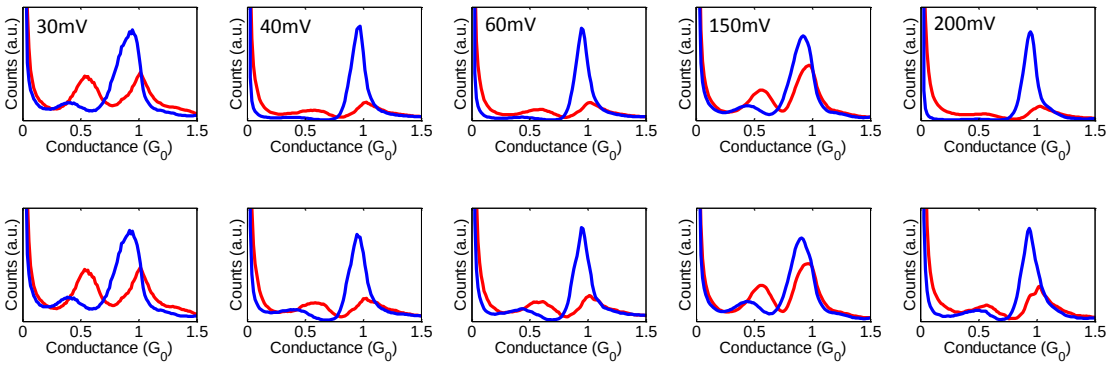

Figure S9. Conductance histograms of Ag/anthracene at different bias voltages. The most probable conductance value extracted from each histogram did not show any dependence on bias voltage up to 200mV. Upper row: Conductance histograms based on full data sets, consisting also traces that do not exhibit any molecular feature. Lower row: The corresponding histograms after automatic trace selection to enhance the visibility of molecular conductance peaks. In these plots only traces with a non-negligible number of conductance counts (typically more than 3-5 points) at the molecular conductance range are presented.

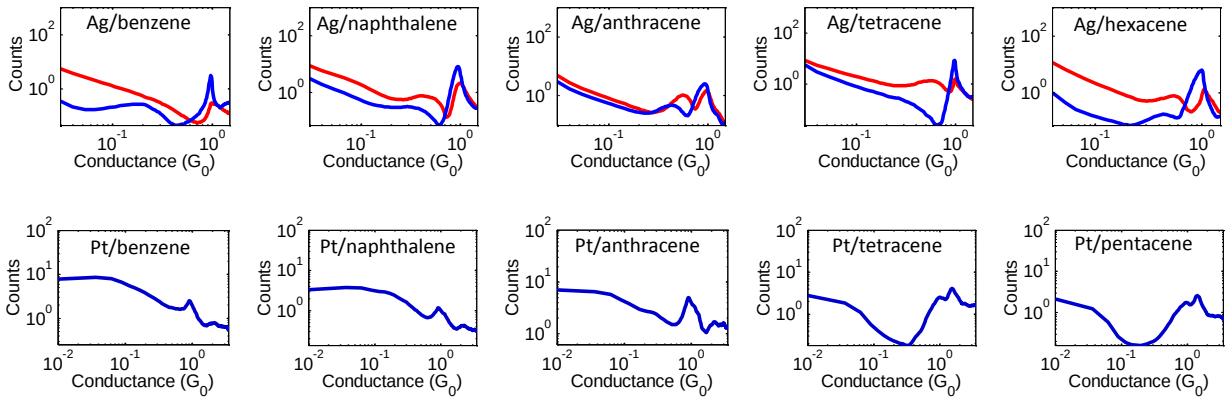

Figure S10. Log-log presentation of conductance histograms for the different molecular junctions. Upper row: histograms of Ag/oligoacene junctions (based on the same trace sets as used for Fig. S7). Lower row: histograms of Pt/oligoacene junctions (based on the same trace sets as used for Fig. S8). All the histograms are based on full data sets without any trace selection.

4. The orbital character of the Pt/oligoacene and Ag/oligoacene hybridization

The different nature of orbital hybridization at the metal-molecule interface for the two types of molecular junctions is revealed in the projected density of states (PDOS) on the last atom of the electrode apices, for Ag and Pt based molecular junctions (Fig. S11). The PDOS of the bare metal atomic junctions are shown for comparison (gray dotted curves). The calculations are performed for the same junction configurations as presented in Fig. 5b. The PDOS of Ag/pentacene (Fig. S11a) shows peaks that do not exist in the PDOS of the bare Ag atomic junction, indicating that the peaks originate from the energy levels of the molecule. In contrast, for Pt/pentacene (Fig. S11b), the presence of the molecule in the junction smears out the *d*-orbitals contribution in the PDOS, which is well pronounced for the bare Pt atomic contact. The molecule induced smearing of the *d*-PDOS indicates a significant orbital hybridization between the *d*-orbitals of the metal and the molecular orbitals. For the Pt based molecular junction, the dominant role of the *d*-orbitals around E_F, which is the energy relevant for electronic transport, is clearly seen in the decomposition of the PDOS into *sp*-character and *d*-character. This can be compared to negligible *d*-contribution around E_F for the Ag based junction. The dominant role of the *d*-orbitals in the case of Pt based junctions is also evident from the characteristic four-lobes shape of the Kohn-Sham eigenfunction of the junction shown in Fig. S11b, Inset. This is in contrast to the eigenfunction of the Ag-based junction, presented in Fig. S11a, Inset, where the *s*-orbital character, with zero nodes, is the dominant one at the metal-molecule interface.

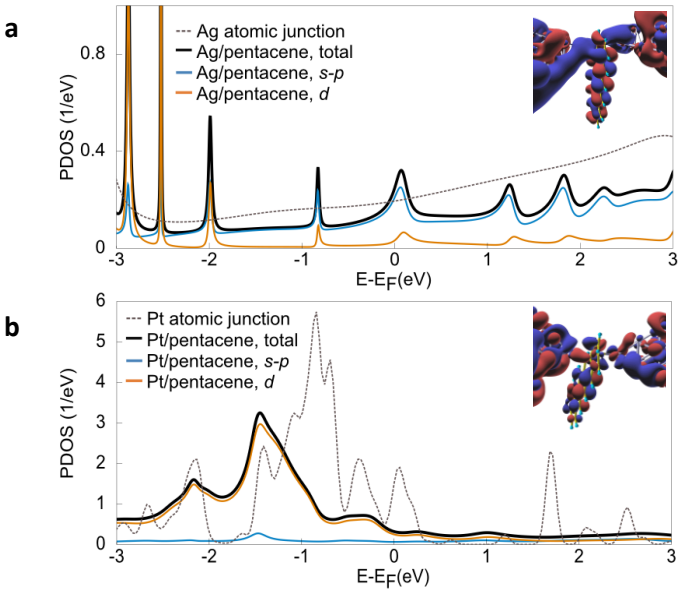

Figure S11. Analysis of the orbital character in the metal-molecule interface. a,b. Projected density of states (PDOS) onto the last atom of the electrodes for pentacene based molecular junctions, and the decomposition into *sp*- and *d*-contributions with **a.** Ag and **b.** Pt electrodes. The PDOS for the bare metal atomic junctions are shown in dotted gray for comparison. **Insets:** representative iso-surfaces of Kohn-Sham eigenfunctions of Ag/pentacene (a) and Pt/pentacene (b) near E_F. The shape of the iso-surfaces and the number of nodes at the electrode-molecule interfaces show the dominant *s*-orbital nature in the first case and the prominent *d*-orbital contribution in the second case. As a side note we point out that although the binding of the molecules to sharp electrodes can be very different from the binding to flat surfaces, the flat-lying geometry of the oligoacene molecule found on flat Ag and Pt surfaces[48–62], translates to the "sandwich compound" compact geometry considered in this paper, where the π-system of the molecules is relatively perpendicular to the axis of the junction.

5. Friedel's sum rule for pedestrians

We consider a molecule coupled to left and right metallic electrodes and demonstrate an explicit relation between the zero-bias conductance and the occupancy of the molecular level. We assume that at low temperatures and zero bias, the electronic transport is governed by a single resonant orbital. Oligoacenes (starting from naphthalene) coupled to Ag electrodes fall into this class, as we demonstrate in the main text with the aid of first-principles calculations. The transmission function $T(\omega)$ is given by

$$T(\omega) = \frac{\Gamma^2}{(\omega-\varepsilon)^2+\Gamma^2} \tag{S1}$$

where ε is the resonance center and 2Γ is the full resonance width at half maximum. The finite width of the resonance is induced by the electrodes, and on writing equation (S1) we assume that the resonant state couples equally to both electrodes. The zero-bias conductance is proportional to the value of the transmission at E_F

$$G = \frac{2e^2}{h}T(E_F) := G_0 T(E_F)$$

Without loss of generality, we set $E_F = 0$. In other words, ε is the resonance center with respect to E_F. The spectral function $A(\omega)$ (density of states) is given by

$$A(\omega) = \frac{1}{\pi}\frac{\Gamma}{(\omega-\varepsilon)^2+\Gamma^2} \tag{S2}$$

The number of electrons in the resonant state is given by integration up to E_F,

$$q = 2\int_{-\infty}^{0} A(\omega)d\omega = 1 - \frac{2}{\pi}arctan\left(\frac{\varepsilon}{\Gamma}\right) = \frac{2}{\pi}arccot\left(\frac{\varepsilon}{\Gamma}\right) \tag{S3}$$

Note the factor of two due to spin degeneracy. We introduce the phase shift

$$cotan(\eta) := \frac{\varepsilon}{\Gamma}, \eta = \frac{\pi}{2}q$$

which allows expressing the conductance as a function of the electron number only,

$$G = G_0\frac{1}{1+\left(\frac{\varepsilon}{\Gamma}\right)^2} = G_0\frac{1}{1+cotan^2(\eta)} = G_0 sin^2(\eta)$$

$$G = G_0 sin^2\left(\frac{\pi}{2}q\right) \tag{S4}$$

If the transport through the molecule in question is dominated by the LUMO, then q represents the number of excess electrons in the LUMO in equilibrium. We note that the total charge transfer may contain components from other orbitals. The relation (S4) is known as Friedel's sum rule for historic reasons. In various forms, it has proven useful in the study of dilute alloys[63], adsorbed molecules[64] and transport through quantum dots[65].

We note here, that this relation holds also in the presence of electron-electron interactions, provided that certain Fermi-liquid identities apply[63,66]. In simpler terms, interactions in the Fermi-liquid state preserve the form of the spectral function and transmission resonance, equations (S1) and (S2), hence the same relation applies. This is the case of normal metallic electrodes at sufficiently low temperatures except for superconducting environments, ferromagnetic environments or other cases with interaction-induced broken symmetries. If the molecule develops a magnetic moment, Friedel's sum rule applies in the low-temperature fully-screened Kondo regime.

6. References

41. Yanson, I. K., Khotkevich, A. V & Krainyukov, S. N. Point-contact spectra and electron-phonon interaction functions of platinum metals. *Phys. Lett. A* **131,** 55–56 (1988).

42. Khotkevich, A. V. & Yanson, I. K. *Atlas of point contact spectra of electron-phonon interactions in metals*. (Springer Science & Business Media, 2013).

43. Lambe, J. & Jaklevic, R. C. Molecular Vibration Spectra by Inelastic Electron Tunneling. *Phys. Rev.* **165,** 821–832 (1968).

44. Djukic, D. *et al.* Stretching dependence of the vibration modes of a single-molecule Pt-H2-Pt bridge. *Phys. Rev. B* **71,** 161402 (2005).

45. Ben-Zvi, R., Vardimon, R., Yelin, T. & Tal, O. Electron–Vibration Interaction in Multichannel Single-Molecule Junctions. *ACS Nano* **7,** 11147–11155 (2013).

46. Troisi, A. & Ratner, M. A. Propensity rules for inelastic electron tunneling spectroscopy of single-molecule transport junctions. *J. Chem. Phys.* **125,** 214709 (2006).

47. Schneebeli, S. T. *et al.* Single-Molecule Conductance through Multiple π−π-Stacked Benzene Rings Determined with Direct Electrode-to-Benzene Ring Connections. *J. Am. Chem. Soc.* **133,** 2136–2139 (2011).

48. Yannoulis, P., Dudde, R., Frank, K. H. & Koch, E. E. Orientation of aromatic hydrocarbons on metal surfaces as determined by NEXAFS. *Surf. Sci.* **189,** 519–528 (1987).

49. Frank, K. H., Yannoulis, P., Dudde, R. & Koch, E. E. Unoccupied molecular orbitals of aromatic hydrocarbons adsorbed on Ag(111). *J. Chem. Phys.* **89,** 7569–7576 (1988).

50. Wolkow, R. A. & Moskovits, M. A comparative study of the electron energy loss spectrum and the surface-enhance Raman spectrum of benzene adsorbed on silver. *J. Chem. Phys.* **96,** 3966–3980 (1992).

51. Guaino, P., Carty, D., Hughes, G., Moriarty, P. & Cafolla, A. A. Scanning tunneling microscopy study of pentacene adsorption on Ag/Si (1 1 1)-(√ 3×√ 3) R30°. *Appl. Surf. Sci.* **212,** 537–541 (2003).

52. Guaino, P. *et al.* Scanning tunnelling spectroscopy of low pentacene coverage on the Ag/Si (111)-(√ 3×√ 3) surface. *J. Phys. Condens. Matter* **15,** S2693 (2003).

53. Huang, W. X. & White, J. M. Growth and Orientation of Naphthalene Films on Ag(111). *J. Phys. Chem. B* **108,** 5060–5065 (2004).

54. Rockey, T. & Dai, H.-L. Adsorbate–substrate bonding and the growth of naphthalene thin films on Ag (111). *Surf. Sci.* **601,** 2307–2314 (2007).

55. Lehwald, S., Ibach, H. & Demuth, J. E. Vibration spectroscopy of benzene adsorbed on Pt(111) and Ni(111). *Surf. Sci.* **78,** 577–590 (1978).

56. Hallmark, V. M., Chiang, S., Brown, J. K. & Wöll, C. Real-space imaging of the molecular organization of naphthalene on Pt(111). *Phys. Rev. Lett.* **66,** 48–51 (1991).

57. Netzer, F. P. Surface structure and reactivity of aromatic molecules: can we track down trends in the periodic table? *Langmuir* **7,** 2544–2547 (1991).

58. Don Norimi, F. & Shirley, C. Calculations of Scanning Tunneling Microscopic Images of Benzene on Pt(111) and Pd(111), and Thiophene on Pd(111). *Jpn. J. Appl. Phys.* **38,** 3809 (1999).

59. Saeys, M., Reyniers, M.-F., Marin, G. B. & Neurock, M. Density functional study of benzene adsorption on Pt (111). *J. Phys. Chem. B* **106,** 7489–7498 (2002).

60. Morin, C., Simon, D. & Sautet, P. Trends in the chemisorption of aromatic molecules on a Pt (111) surface: benzene, naphthalene, and anthracene from first principles calculations. *J. Phys. Chem. B* **108,** 12084–12091 (2004).

61. Morin, C., Simon, D. & Sautet, P. Chemisorption of Benzene on Pt(111), Pd(111), and Rh(111) Metal Surfaces: A Structural and Vibrational Comparison from First Principles. *J. Phys. Chem. B* **108,** 5653–5665 (2004).

62. Montano, M., Salmeron, M. & Somorjai, G. A. STM studies of cyclohexene hydrogenation/dehydrogenation and its poisoning by carbon monoxide on Pt (111). *Surf. Sci.* **600,** 1809–1816 (2006).

63. Hewson, A. C. *The Kondo problem to heavy fermions* . (Cambridge university press, 1997).

64. Desjonqueres, M.-C. *Concepts in Surface Physics: 2ème édition*. **30,** (Springer Science & Business Media, 1996).

65. Pustilnik, M. & Glazman, L. Kondo effect in quantum dots. *J. Phys. Condens. Matter* **16,** R513 (2004).

66. Langer, J. S. & Ambegaokar, V. Friedel Sum Rule for a System of Interacting Electrons. *Phys. Rev.* **121,** 1090–1092 (1961).